

Superbroadband near-IR photoluminescence from Pr³⁺-doped fluorotellurite glasses

Bo Zhou,^{1,3,4} Lili Tao,² Yuen H. Tsang,^{2,5} Wei Jin,³ and Edwin Yue-Bun Pun¹

¹Department of Electronic Engineering, City University of Hong Kong, Tat Chee Avenue, Kowloon, Hong Kong

²Department of Applied Physics and Materials Research Center, The Hong Kong Polytechnic University, Hung Hom, Kowloon, Hong Kong

³Department of Electrical Engineering, The Hong Kong Polytechnic University, Hung Hom, Kowloon, Hong Kong

⁴eebzhou@polyu.edu.hk

⁵Yuen.Tsang@polyu.edu.hk

Abstract: Praseodymium(Pr³⁺)-doped fluorotellurite glasses were synthesized and broadband photoluminescence (PL) covering a wavelength range from 1.30 to 1.67 μm was observed under both 488 and 590 nm wavelength excitations. The broadband PL emission is mainly due to the radiative transition from the manifolds Pr³⁺: ¹D₂ to ¹G₄. The PL line-shape, band width, and lifetime were modified by the Pr³⁺ dopant concentration, and a quantum efficiency as high as 73.7% was achieved with Pr³⁺ dopant in a low concentration of 0.05 mol%. The good spectroscopic properties were also predicted by the Judd-Ofelt analysis, which indicates a stronger asymmetry and covalent bonding between the Pr³⁺ sites and the matrix ligand field. The large stimulated emission cross-section, long measured lifetime, and broad emission bandwidth confirm the potential of the Pr³⁺-singly doped fluorotellurite glass as broadband luminescence sources for the broadband near-infrared optical amplifications and tunable lasers.

©2012 Optical Society of America

OCIS codes: (160.5690) Rare-earth-doped materials; (300.6280) Spectroscopy, fluorescence and luminescence; (230.2285) Fiber devices and optical amplifiers.

References and links

1. G. A. Thomas, B. I. Shraiman, P. F. Glodis, and M. J. Stephen, "Towards the clarity limit in optical fibre," *Nature* **404**(6775), 262–264 (2000).
2. S. Kasap, "Optoelectronics," in *The Optics Encyclopedia*, T. Brown, K. Creath, H. Kogelnik, M. A. Kriss, J. Schmit, and M. J. Weber, eds. (Wiley-VCH, Weinheim, Germany, 2004), Vol. 4., pp. 2237–2284.
3. See, for example, M. J. F. Digonnet, ed., *Rare-Earth-Doped Fiber Lasers and Amplifiers* (Second Edition, Revised and Expanded), (Marcel Dekker, New York, 2009), and references therein.
4. H. Takebe, K. Yoshino, T. Murata, K. Morinaga, J. Hector, W. S. Brocklesby, D. W. Hewak, J. Wang, and D. N. Payne, "Spectroscopic properties of Nd³⁺ and Pr³⁺ in gallate glasses with low phonon energies," *Appl. Opt.* **36**(24), 5839–5843 (1997).
5. M. Naftaly, S. Shen, and A. Jha, "Tm³⁺-doped tellurite glass for a broadband amplifier at 1.47 μm," *Appl. Opt.* **39**(27), 4979–4984 (2000).
6. B. Zhou, H. Lin, D. Yang, and E. Y. B. Pun, "Emission of 1.38 μm and gain properties from Ho³⁺-doped low-phonon-energy gallate bismuth lead oxide glasses for fiber-optic amplifiers," *Opt. Lett.* **35**(2), 211–213 (2010).
7. C. Strohhofer and A. Polman, "Silver as a sensitizer for erbium," *Appl. Phys. Lett.* **81**(8), 1414–1416 (2002).
8. K. Driesen, V. K. Tikhomirov, C. Görller-Walrand, V. D. Rodriguez, and A. B. Seddon, "Transparent Ho³⁺-doped nano-glass-ceramics for efficient infrared emission," *Appl. Phys. Lett.* **88**(7), 073111 (2006).
9. J. Dong, Y. Q. Wei, A. Wonfor, R. V. Penty, I. H. White, J. Lousteau, G. Jose, and A. Jha, "Dual-pumped tellurite fiber amplifier and tunable laser using Er/Ce codoping scheme," *IEEE Photon. Technol. Lett.* **23**(11), 736–738 (2011).
10. S. Tanabe, "Rare-earth-doped glasses for fiber amplifiers in broadband telecommunication," *C. R. Chim.* **5**(12), 815–824 (2002).
11. S. Y. Seo, J. H. Shin, B. S. Bae, N. Park, J. J. Penninkhof, and A. Polman, "Erbium-thulium interaction in broadband infrared luminescent silicon-rich silicon oxide," *Appl. Phys. Lett.* **82**(20), 3445–3447 (2003).
12. L. Huang, A. Jha, S. Shen, and X. Liu, "Broadband emission in Er³⁺-Tm³⁺ codoped tellurite fibre," *Opt. Express* **12**(11), 2429–2434 (2004).
13. Z. Xiao, R. Serna, C. N. Afonso, and I. Vickridge, "Broadband infrared emission from Er-Tm:Al₂O₃ thin films," *Appl. Phys. Lett.* **87**(11), 111103 (2005).

14. D. Chen, Y. Wang, F. Bao, and Y. Yu, "Broadband near-infrared emission from Tm³⁺/Er³⁺ co-doped nanostructured glass ceramics," *J. Appl. Phys.* **101**(11), 113511 (2007).
15. Y. Xu, Q. Zhang, C. Shen, D. Chen, H. Zeng, and G. Chen, "Broadband near-IR emission in Tm/Er-codoped GeS₂-In₂S₃-based chalcogenide glasses," *J. Am. Ceram. Soc.* **92**(12), 3088–3091 (2009).
16. B. Zhou and E. Y. B. Pun, "Broadband near-infrared photoluminescence and energy transfer in Tm³⁺/Er³⁺ codoped low phonon energy gallate bismuth lead glasses," *J. Phys. D Appl. Phys.* **44**(28), 285404 (2011).
17. K. Murata, Y. Fujimoto, T. Kanabe, H. Fujita, and M. Nakatsuka, "Bi-doped SiO₂ as a new laser material for an intense laser," *Fusion Eng. Des.* **44**(1-4), 437–439 (1999).
18. M. Y. Sharonov, A. B. Bykov, V. Petricevic, and R. R. Alfano, "Spectroscopic study of optical centers formed in Bi-, Pb-, Sb-, Sn-, Te-, and In-doped germanate glasses," *Opt. Lett.* **33**(18), 2131–2133 (2008).
19. V. G. Truong, L. Bigot, A. Lerouge, M. Douay, and I. Razzobreev, "Study of thermal stability and luminescence quenching properties of bismuth-doped silicate glasses for fiber laser applications," *Appl. Phys. Lett.* **92**(4), 041908 (2008).
20. M. A. Hughes, T. Akada, T. Suzuki, Y. Ohishi, and D. W. Hewak, "Ultrabroad emission from a bismuth doped chalcogenide glass," *Opt. Express* **17**(22), 19345–19355 (2009).
21. B. Wu, S. Zhou, J. Ruan, Y. Qiao, D. Chen, C. Zhu, and J. Qiu, "Enhanced near-infrared emission from Ni²⁺ in Cr³⁺/Ni²⁺ codoped transparent glass ceramics," *Appl. Phys. Lett.* **92**(15), 151102 (2008).
22. I. A. Bufetov and E. M. Dianov, "Bi-doped fiber lasers," *Laser Phys. Lett.* **6**(7), 487–504 (2009).
23. N. D. Psaila, R. R. Thomson, H. T. Bookey, A. K. Kar, N. Chiodo, R. Osellame, G. Cerullo, G. Brown, A. Jha, and S. Shen, "Femtosecond laser inscription of optical waveguides in Bismuth ion doped glass," *Opt. Express* **14**(22), 10452–10459 (2006).
24. M. Peng, G. Dong, L. Wondraczek, L. Zhang, N. Zhang, and J. Qiu, "Discussion on the origin of NIR emission from Bi-doped materials," *J. Non-Cryst. Solids* **357**(11–13), 2241–2245 (2011).
25. B. Zhou, H. Lin, and E. Y. B. Pun, "Tm³⁺-doped tellurite glasses for fiber amplifiers in broadband optical communication at 1.20 μm wavelength region," *Opt. Express* **18**(18), 18805–18811 (2010).
26. B. Zhou, H. Lin, B. Chen, and E. Y. B. Pun, "Superbroadband near-infrared emission in Tm-Bi codoped sodium-germanium-gallate glasses," *Opt. Express* **19**(7), 6514–6523 (2011).
27. Y. G. Choi, K. H. Kim, B. J. Park, and J. Heo, "1.6 μm emission from Pr³⁺: (³F₃, ³F₄) → ³H₄ transition in Pr³⁺- and Pr³⁺/Er³⁺-doped selenide glasses," *Appl. Phys. Lett.* **78**(9), 1249–1251 (2001).
28. B. Zhou and E. Y. B. Pun, "Superbroadband near-IR emission from praseodymium-doped bismuth gallate glasses," *Opt. Lett.* **36**(15), 2958–2960 (2011).
29. P. Nandi, G. Jose, C. Jayakrishnan, S. Debbarma, K. Chalpathi, K. Alti, A. K. Dharmadhikari, J. A. Dharmadhikari, and D. Mathur, "Femtosecond laser written channel waveguides in tellurite glass," *Opt. Express* **14**(25), 12145–12150 (2006).
30. B. Zhou, E. Y. B. Pun, H. Lin, D. Yang, and L. Huang, "Judd-Ofelt analysis, frequency upconversion, and infrared photoluminescence of Ho³⁺-doped and Ho³⁺/Yb³⁺-codoped lead bismuth gallate oxide glasses," *J. Appl. Phys.* **106**(10), 103105 (2009).
31. M. Naftaly, C. Batchelor, and A. Jha, "Pr³⁺-doped fluoride glass for a 589 nm fiber laser," *J. Lumin.* **91**(3-4), 133–138 (2000).
32. A. Jha, S. Shen, and M. Naftaly, "Structural origin of spectral broadening of 1.5-μm emission in Er³⁺-doped tellurite glasses," *Phys. Rev. B* **62**(10), 6215–6227 (2000).
33. R. Jose, Y. Arai, and Y. Ohishi, "Raman scattering characteristics of the TBSN-based tellurite glass system as a new Raman gain medium," *J. Opt. Soc. Am. B* **24**(7), 1517–1526 (2007).
34. V. Nazabal, S. Todoroki, A. Nukui, T. Matsumoto, S. Suehara, T. Hondo, T. Araki, S. Inoue, C. Rivero, and T. Cardinal, "Oxyfluoride tellurite glasses doped by erbium: thermal analysis, structural organization and spectral properties," *J. Non-Cryst. Solids* **325**(1-3), 85–102 (2003).
35. G. Liao, Q. Chen, J. Xing, H. Gebavi, D. Milanese, M. Fokine, and M. Ferraris, "Preparation and characterization of new fluorotellurite glasses for photonic application," *J. Non-Cryst. Solids* **355**(7), 447–452 (2009).
36. A. Lin, A. Rysanyanskiy, and J. Toulouse, "Fabrication and characterization of a water-free mid-infrared fluorotellurite glass," *Opt. Lett.* **36**(5), 740–742 (2011).
37. B. R. Judd, "Optical absorption intensities of rare-earth ions," *Phys. Rev.* **127**(3), 750–761 (1962).
38. G. S. Ofelt, "Intensities of crystal spectra of rare-earth ions," *J. Chem. Phys.* **37**(3), 511–520 (1962).
39. W. T. Carnall, P. R. Fields, and K. Rajnak, "Electronic energy levels in the trivalent lanthanide aquo ions. I. Pr³⁺, Nd³⁺, Pm³⁺, Sm³⁺, Dy³⁺, Ho³⁺, Er³⁺, and Tm³⁺," *J. Chem. Phys.* **49**(10), 4424–4442 (1968).
40. R. T. Génova, I. R. Martín, U. R. Rodríguez-Mendoza, F. Lahoz, A. D. Lozano-Gorrin, P. Nunez, J. Gonzalez-Platas, and V. Lavin, "Optical intensities of Pr³⁺ ions in transparent oxyfluoride glass and glass-ceramic. Applications of the standard and modified Judd-Ofelt theories," *J. Alloy. Comp.* **380**(1-2), 167–172 (2004).
41. L. R. Moorthy, M. Jayasimhadri, A. Radhapathy, and R. V. S. S. N. Ravikumar, "Lasing properties of Pr³⁺-doped tellurofluorophosphate glasses," *Mater. Chem. Phys.* **93**(2-3), 455–460 (2005).
42. M. A. Newhouse, R. F. Bartholomew, B. G. Aitken, L. J. Button, and N. F. Borrelli, "Pr-doped mixed-halide glasses for 1300 nm amplification," *IEEE Photon. Technol. Lett.* **6**(2), 189–191 (1994).
43. M. J. Weber, "Spontaneous emission probabilities and quantum efficiencies for excited states of Pr³⁺ in LaF₃," *J. Chem. Phys.* **48**(10), 4774–4780 (1968).
44. T. Suzuki, G. S. Murugan, and Y. Ohishi, "Optical properties of transparent Li₂O-Ga₂O₃-SiO₂ glass-ceramics embedding Ni-doped nanocrystals," *Appl. Phys. Lett.* **86**(13), 131903 (2005).
45. M. Peng, J. Qiu, D. Chen, X. Meng, and C. Zhu, "Superbroadband 1310 nm emission from bismuth and tantalum codoped germanium oxide glasses," *Opt. Lett.* **30**(18), 2433–2435 (2005).

1. Introduction

Recently, the expansion of the transmission window of silica fibers to a broader range of 1.2–1.7 μm makes it attractive to explore superbroadband luminescence sources for the broadband near-infrared (IR) optical amplifiers and tunable lasers operating in this expanded low loss window [1,2]. Early investigations have demonstrated that rare earth ions of erbium (Er^{3+}), thulium (Tm^{3+}), holmium (Ho^{3+}), and praseodymium (Pr^{3+}) are good candidates for the optical amplifications at separate C-, L-, S-, E-, and O-bands in this expanded window, and considerable progress have been achieved [3]. To further improve the quantum efficiency, novel low phonon energy host (e.g., heavy metal oxide glasses and transparent glass-ceramics), rare earths codoping schemes (e.g., Er^{3+} - Ce^{3+} for the C-band optical amplification), dual-pump configuration, and nano-structures (e.g., silver nanoparticles) have been investigated [4–10]. The codoping scheme has been also demonstrated to be an effective approach to achieve broader emission, and broadband near-IR emission covering S + L-band has already been obtained in Er^{3+} - Tm^{3+} codoped systems [11–16]. On the other hand, broadband near-IR luminescence peaking around 1.3 μm from the transition metal (TM) and heavy metal (HM) ions such as active bismuth (Bi), nickel (Ni), chromium (Cr), and lead (Pb) were investigated [17–23], and their fiber/waveguide applications have been explored [22,23], although the luminescence origins for some of them (e.g., Bi^+ and/or Bi^{5+}) need further studies [24]. We have recently observed the broadband emissions around 1.20 and 1.47 μm wavelengths in Tm^{3+} -singly doped tellurite glass under blue wavelength excitation [25,26], and further achieved the superbroadband near-IR luminescence covering 1.0–1.7 μm wavelength region from Tm-Bi codoped gallogermanate glasses taking advantage of Bi emissions located around 1.3 μm .

Among the rare earth ions, Pr^{3+} shows potential to yield luminescence at specific near-IR wavelength bands within the expanded low loss window considering its rich multiple energy levels. Apart from the 1.3 μm emission (Pr^{3+} : $^1\text{G}_4 \rightarrow ^3\text{H}_5$) [10], an intense emission located at 1.6 μm from the Pr^{3+} : $^3\text{F}_{4,3} \rightarrow ^3\text{H}_4$ transition was also obtained in selenide glasses [27], which presents a promising candidate for the U-band optical amplification. We recently observed the superbroadband near-IR luminescence from Pr^{3+} -singly doped bismuth gallate glasses [28]. However, the relatively stronger intrinsic absorption of the bismuth gallate glass at the short wavelength side (<500 nm) would result in a serious depression of the blue light pump efficiency. To overcome it, development of host matrix with higher transmission at blue wavelength region together with unique ligand field is necessary.

In this work, we report the observation of broadband near-IR luminescence extended from 1.30 to 1.67 μm in Pr^{3+} -singly doped novel fluorotellurite glasses for the first time to our best knowledge. Tellurite-based glasses show high refractive index, low phonon energy, good mechanical properties and chemical durability [5,25]. More significantly, near-IR tellurite glass fiber/waveguide amplifiers and lasers have been reported [9,12,29]. Some of fluorides were added to modify the local ligand field between the Pr^{3+} and the host matrix. The high transparency at the short wavelength side (<500 nm) enables to improve the pump efficiency under blue excitation sources. The energy transfer processes involved are proposed and discussed, and the optical amplification is also evaluated.

2. Experimental

Pr^{3+} -doped fluorotellurite glass samples were prepared by melting the well-mixed batches of high-purity chemicals with mol% composition of 3LaF_3 - 4BaF_2 - 4BaCO_3 - 9ZnO - 80TeO_2 - $x\text{PrF}_3$ ($x=0.05, 0.1, 0.3, 0.5, \text{ and } 1.0$) following the procedures described in Ref [25]. For comparison, a sample without Pr^{3+} doping was also prepared. The as-prepared glasses were cut and optically polished for optical measurements. The refractive indices of the glass samples were measured using a Metricon 2010 prism coupler and they are 2.068 and 2.013 at wavelengths of 632.8 and 1536 nm. The profile of the indices on wavelength was determined to be $n(\lambda) = 2.002 + 26333.26/\lambda^2$ (the wavelength λ is in unit of nm) using Cauchy formula [30]. The Raman spectrum of undoped glass sample was measured by a HORIBA Jobin Yvon

HR800 Raman spectrometer with a 488 nm laser excitation source. The absorption spectra were recorded using a Perkin Elmer UV-VIS-NIR Lambda 19 double beam spectrophotometer. The visible and infrared photoluminescence (PL) spectra were recorded using a photomultiplier tube (PMT) and a near-IR PMT detector, respectively. The excitation sources were tuned from a continuous xenon lamp by a monochromator. The photoluminescence excitation (PLE) spectra were recorded using the same setup with a continuous wavelength xenon lamp as the excitation source. The emission decay curves were recorded using the same setup with a flash xenon lamp as the excitation source. All the measurements were carried out at room temperature.

3. Results and discussion

Figure 1 shows the optical absorption spectrum of the 0.5 mol% Pr³⁺-doped glass sample. Absorption bands located at 447, 472, 485, 592, 1018, 1448, 1543, 1951, and 2331 nm are assigned to the transitions from the ground state ³H₄ to specific excited states ³P₂, ¹I₆ + ³P₁, ³P₀, ¹D₂, ¹G₄, ³F₄, ³F₃, ³F₂, and ³H₆, respectively. There are broad and intense absorption bands in 440-490 nm wavelength region, as shown in inset (a) of Fig. 1. This is different from that in bismuth gallate glass where only a very weak absorption band corresponding to the ³P₀ was recorded in this wavelength region [28]. The higher transparency of fluorotellurite glass than the bismuth gallate glass in short wavelength side would enable to get more efficient emission under the blue light excitations. The absorption cross-section which determines the absorption efficiency of the active ions on the pump sources can be calculated by $\sigma_{abs}(\lambda) = 2.303E(\lambda)/Nd$, where N , d , and $E(\lambda)$ represent the ion density, the thickness, and the absorbance of the substrate glass, respectively. For instance, σ_{abs} was obtained to be 1.43×10^{-20} cm² for the ³P₀ absorption band, this value is much larger than that of Pr³⁺ in fluoroaluminate and ZBLAN glasses [31].

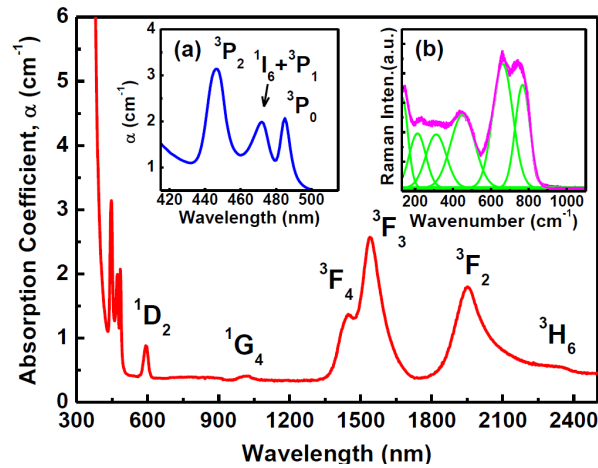


Fig. 1. Optical absorption spectrum of (0.5 mol%)Pr³⁺-doped fluorotellurite glass. Inset (a) shows the detail of the absorption bands corresponding to the manifolds (³P₂, ¹I₆+³P₁, ³P₀); Inset (b) shows the Raman spectrum (pink line) of undoped fluorotellurite glass with Gaussian fitting (green lines).

The inset (b) of Fig. 1 shows the Raman spectrum of the undoped host measured using a 488 nm laser excitation. The maximum phonon energy is determined to be ~766 cm⁻¹ by Gaussian fitting, which can be assigned to the stretching vibrations of TeO_{3+δ} polyhedral, and/or tellurium and non-bridging oxygen atoms in TeO₃ trigonal pyramid units [32,33]. This value is comparable to many other oxide-based tellurite and fluorotellurite glasses [32–36]. The band with the most intense peak at 658 cm⁻¹ is due to the anti-symmetric vibration modes of TeO₄, and the bands in lower frequency region at 311 and 451 cm⁻¹ can be attributed to the

bending vibration bonds of O-Te-O/Te-O-Te linkages of TeO₄ [34]. The Raman spectrum intensity of the peak at 658 cm⁻¹ in comparison to that at ~766 cm⁻¹ in fluorotellurite glass is slightly lower than those of the oxide-based tellurite glasses, this may be ascribed to the breakage effect of F ions on Te-O bonds and/or formation of more TeO_{3+δ}/Te(O,F)_{3+δ} groups [34–36]. This indicates that fluorides play a different role as network modifiers in comparison to the oxides.

A Judd-Ofelt analysis can be performed to predict the spontaneous transition properties of Pr³⁺ in host matrix [37,38]. In the present work, absorption bands (³P₂, ³P₁+¹I₆, ³P₀, ¹D₂, ¹G₄, ³F₄, ³F₃, ³F₂, and ³H₆,) were used for the Judd-Ofelt calculation, and the overlapped bands were de-convoluted using Gaussian fitting. The reduced matrix elements of the tensor operators used in the calculation of the electric dipole line strengths (*S_{ed}*) can be considered independent of the host materials and the values of them were quoted from Ref [39]. The phenomenological Judd-Ofelt intensity parameters Ω_{*t*} (*t*=2,4,6) were calculated by a least-squares fitting of the electric dipole oscillator strengths from the experiment (*P_{exp}*) and calculation (*P_{cal}*). The root-mean-square deviation δ_{*rms*} between the *P_{exp}* and *P_{cal}* was calculated by $\delta_{rms} = \left[\sum (P_{exp} - P_{cal})^2 / (N_{tran} - N_{para}) \right]^{1/2}$, where *N_{tran}* and *N_{para}* are the number of the transition and parameters used in the calculation. The Ω_{*t*} (*t*=2,4,6) are obtained to be (3.57, 6.60, 5.18)×10⁻²⁰ cm², and δ_{*rms*} is obtained to be 3.54×10⁻⁶. The percentage error of the Judd-Ofelt analysis is 39.4%. The measured and the calculated oscillator strength values are shown in Table 1. Generally, the asymmetry of the local structure and the covalency of the lanthanide-ligand bonds can be reflected by the Ω₂. The Ω₂ value of Pr³⁺ in fluorotellurite glass is much larger in comparison to that in transparent oxyfluoride glass and glass ceramics, tellurofluorophosphate glass, fluorozirconate and mix-halide glasses [40–42], indicating a stronger asymmetry and covalent environment between the Pr³⁺ ions and the ligand in the fluorotellurite glass matrix than in those host.

Table 1. Measured and calculated oscillator strengths, and electric dipole line strengths of absorption transitions of Pr³⁺ in fluorotellurite glass

Absorption band	Energy (cm ⁻¹)	Refractive index	<i>P_{exp}</i> (×10 ⁻⁶)	<i>P_{cal}</i> (×10 ⁻⁶)	<i>S_{ed}</i> (×10 ⁻²⁰)
³ H ₄ → ³ P ₂	22384	2.1342	14.041	5.684	0.941
³ H ₄ → ¹ I ₆ + ³ P ₁	21185	2.1204	9.771	9.186	1.626
³ H ₄ → ³ P ₀	20624	2.1142	4.910	6.245	1.414
³ H ₄ → ¹ D ₂	16863	2.0771	3.436	1.696	3.910
³ H ₄ → ¹ G ₄	9850	2.0278	0.409	0.461	1.897
³ H ₄ → ³ F ₄	6981	2.0151	4.543	4.961	2.910
³ H ₄ → ³ F ₃	6497	2.0134	9.668	9.735	0.614
³ H ₄ → ³ F ₂	5126	2.0092	6.357	6.343	0.509
³ H ₄ → ³ H ₆	4328	2.0072	0.515	0.988	0.941

Using Ω_{*t*} (*t*=2,4,6) values, the spontaneous transition probability (*A*), originating from an electrical dipole transition from *aJ* to *bJ'* can be calculated by

$$A(aJ;bJ') = \frac{64\pi^4 e^2}{3h\lambda^3 (2J+1)} \frac{n(n^2+2)^2}{9} \times S_{ed}(aJ;bJ'), \quad (1)$$

where *e* is the charge of electron, *h* is the Planck constant, *n* is the refractive index, λ is the wavelength of the transition, and *J* is the total angular momentum quantum number. The matrix elements used in calculation of *S_{ed}* (*aJ*;*bJ'*) in Eq. (1) are employed from Ref [43]. The spontaneous transition probability from magnetic contribution can be ignored because they are

very small compared with the electrical dipole transition. And other important parameters including the branch ratio $\beta(aJ;bJ')$ and radiative lifetime τ_{rad} can be further calculated by $\beta(aJ;bJ') = A(aJ;bJ') / \sum_{J'} A(aJ;bJ')$ and $\tau_{rad} = 1 / \sum_{J'} A(aJ;bJ')$, where the summation is over all transitions to every terminal state bJ' . The radiative quantum efficiency η is defined as $\eta = \tau_m / \tau_{rad}$, where τ_m is the measured lifetime. The results for transitions from Pr^{3+} : $^3\text{P}_1$, $^3\text{P}_0$, $^1\text{D}_2$, and $^1\text{G}_4$ in fluorotellurite glass are summarized in Table 2. The transition probability for the Pr^{3+} : $^1\text{D}_2 \rightarrow ^1\text{G}_4$ is 880.1^{-1} with a branch ratio of 11.05%. And for the $^3\text{P}_0$, most of the energy in this level would radiate to the ground-state, this is in agreement with the experimental observations where the blue emission ($^3\text{P}_0 \rightarrow ^3\text{H}_4$) dominates [41,42].

Table 2. Spontaneous transition parameters of Pr^{3+} : $^3\text{P}_1$, $^3\text{P}_0$, $^1\text{D}_2$, and $^1\text{G}_4$ in fluorotellurite glass

aJ	bJ'	Energy (cm^{-1})	A (s^{-1})	β (%)	τ_{rad} (μs)		
$^3\text{P}_1$	$^3\text{P}_0$	561	0	0	2.9		
	$^1\text{D}_2$	4322	11.5	0.03			
	$^1\text{G}_4$	11335	3266.5	9.59			
	$^3\text{F}_4$	14204	3140	9.22			
	$^3\text{F}_3$	14668	6170.1	18.11			
	$^3\text{F}_2$	16059	2385.7	7.00			
	$^3\text{H}_6$	16857	1871.5	5.49			
	$^3\text{H}_5$	19021	10149.9	29.80			
	$^3\text{H}_4$	21185	7067.4	20.76			
	$^3\text{P}_0$	$^1\text{D}_2$	3761	14.88		0.01	8.2
$^1\text{G}_4$		10774	2157.4	1.77			
$^3\text{F}_4$		13643	12927.7	10.60			
$^3\text{F}_3$		14127	0	0			
$^3\text{F}_2$		15498	25522.1	20.92			
$^3\text{H}_6$		16296	10739.6	8.81			
$^3\text{H}_5$		18461	0	0			
$^3\text{H}_4$		20624	70614	57.89			
$^1\text{D}_2$		$^1\text{G}_4$	7013	880.1	11.05	125.5	
		$^3\text{F}_4$	9882	2254	28.29		
	$^3\text{F}_3$	10366	297.6	3.74			
	$^3\text{F}_2$	11737	979	12.29			
	$^3\text{H}_6$	12535	1132.6	14.21			
	$^3\text{H}_5$	14701	59.6	0.75			
	$^3\text{H}_4$	16863	2364.7	29.67			
$^1\text{G}_4$	$^3\text{F}_4$	2869	38.5	2.68	695.5		
	$^3\text{F}_3$	3353	6.5	0.45			
	$^3\text{F}_2$	4724	11.2	0.78			
	$^3\text{H}_6$	5522	321.7	22.37			
	$^3\text{H}_5$	7688	997.3	69.35			
	$^3\text{H}_4$	9850	62.8	4.37			

Figure 2(a) shows the near-IR PL spectra of Pr^{3+} -doped samples under 488 nm excitation. Broadband emissions covering 1.30-1.67 μm wavelength region are observed for the samples with lower Pr^{3+} dopant concentration. With the increasing of Pr^{3+} , the PL intensity decreases after an initial increase, and the emission peak extends to the short wavelength side whilst the

emission band at the long wavelength side declines. Figure 2(b) shows the full-width at half-maximum (FWHM) of the emission bands. It can be seen that the FWHM increases with the increasing of Pr^{3+} and reaches a maximum FWHM bandwidth of 196 nm when Pr^{3+} concentration is equal to 1.0 mol%. This broadband emission can be assigned to the Pr^{3+} : $^1\text{D}_2 \rightarrow ^1\text{G}_4$ transition, the unique ligand of the Pr^{3+} sites in the fluorotellurite matrix enables the observation of broadband emission from this transition. The emission band at the shorter wavelength side might be also contributed by the Pr^{3+} : $^1\text{G}_4 \rightarrow ^3\text{H}_5$ transition [23]. In deed, an intense emission at around 1.33 μm corresponding to this transition is observed under 996 nm wavelength excitation [see Fig. 2(c)]. The PL intensity decline at higher Pr^{3+} doping level, in particular, at the longer wavelength side can be ascribed to the cross relaxation processes [$^1\text{D}_2$, $^3\text{H}_4 \rightarrow ^1\text{G}_4$, $^3\text{F}_{4,3}$], considering the spectral overlap of the emission band ($^1\text{D}_2 \rightarrow ^1\text{G}_4$) and the absorption band ($^3\text{F}_{4,3} \leftarrow ^3\text{H}_4$) as shown in Fig. 2(c). The closer Pr^{3+} - Pr^{3+} separation at higher Pr^{3+} doping level makes this process occur easily, leading to a depleting of the emission level Pr^{3+} : $^1\text{D}_2$ [28].

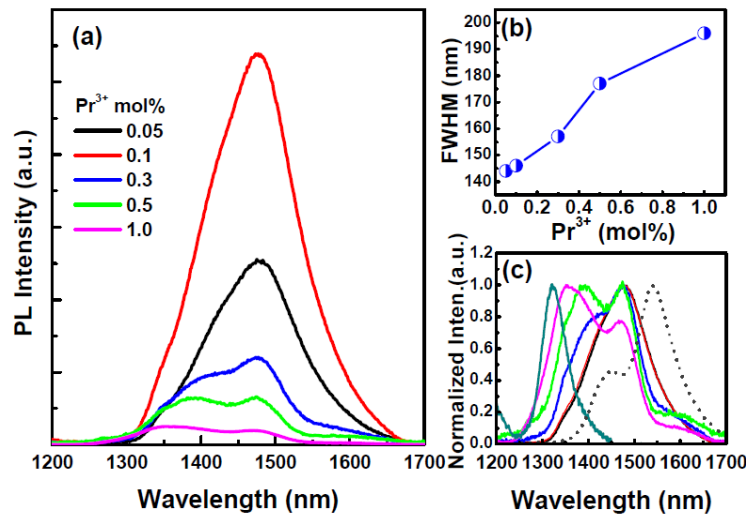


Fig. 2. (a) Near-IR PL spectra of Pr^{3+} -doped fluorotellurite glasses under 488 nm wavelength excitation. (b) The FWHM bandwidth of the emissions at different Pr^{3+} dopant concentration. (c) Normalized PL spectra line-shapes and a comparison of them with the Pr^{3+} : $^3\text{F}_{4,3} \leftarrow ^3\text{H}_4$ absorption band (dotted line) located in this wavelength region. The 1.33 μm emission from the Pr^{3+} : $^1\text{G}_4 \rightarrow ^3\text{H}_5$ transition is also displayed in Fig. 2(c).

To optimize the excitation wavelengths, the PLE spectra were measured at 1480 nm and are shown in Fig. 3(a). It can be seen that, apart from the excitation at around 590 nm, broad excitation bands extending from 440 to 490 nm also have contributions to the near-IR emission. The excitation band corresponds to the manifolds ($^3\text{P}_{0,1,2}$, $^1\text{I}_6$), on which the energy can decay rapidly to the next lower emission level $^1\text{D}_2$ mainly through the cross relaxation [$^3\text{P}_0$, $^3\text{H}_4 \rightarrow ^1\text{D}_2$, ($^3\text{H}_6$, $^3\text{F}_2$)]; the radiative decay can be ignored because the $^3\text{P}_0 \rightarrow ^1\text{D}_2$ transition rate is very low according to the Judd-Ofelt result. It can be also found that this excitation band exhibits similar change compared with the near-IR PL spectra as the Pr^{3+} concentration increases whilst the excitation band ($^3\text{P}_{0,1,2}$, $^1\text{I}_6$) gives a relatively rapider decrease in comparison to the 590 nm ($^1\text{D}_2$) excitation band [see Fig. 3(a)]. The excitation band around 590 nm shows advantage, in particular, at higher Pr^{3+} dopant concentration, is primarily due to the resonant excitation route by which the emission level Pr^{3+} : $^1\text{D}_2$ is populated directly.

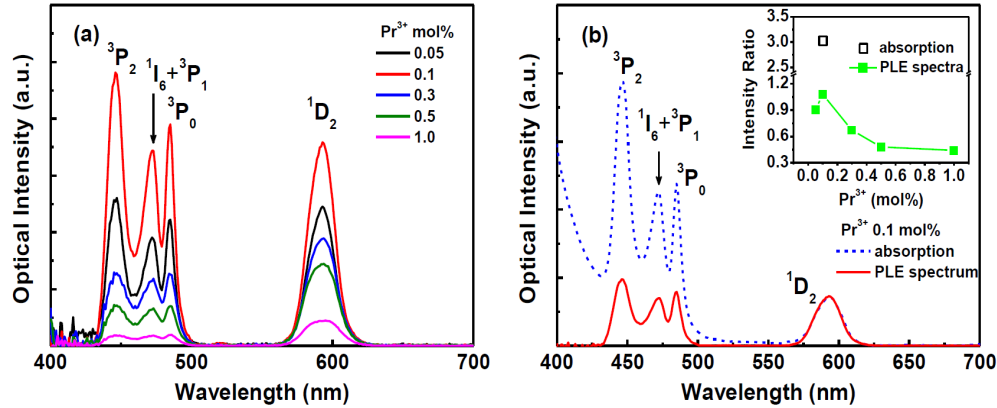


Fig. 3. (a) PLE spectra of Pr^{3+} -doped fluorotellurite glass samples monitored at 1480 nm. (b) A comparison of the PLE spectrum and the absorption spectrum with respect to the 590 nm band for the 0.1 mol% Pr^{3+} -doped sample. Inset of (b) shows the absorption/PLE spectra intensity ratio of the ${}^3\text{P}_0$ band to the ${}^1\text{D}_2$ band.

By comparing the PLE spectra with the absorption spectrum [see Fig. 3(b) and the inset], it can be found that the absorptions in 440-490 nm wavelength region with respect to the 590 nm band is much more intense than that in the PLE spectra. This result indicates that there are some other decays for the energy residing in the (${}^3\text{P}_{0,1,2}, {}^1\text{I}_6$) manifolds. To further understand this phenomenon, the visible PL spectra under 445 nm excitation were recorded and are shown in Fig. 4. It should be mentioned that there is no obvious change in the near-IR emission line-shapes measured under 445 nm compared with those measured under 488 nm wavelength excitation. Intense visible emissions peaking around 490, 528, 611, and 643 nm are observed, and they were assigned to the Pr^{3+} : ${}^3\text{P}_0 \rightarrow {}^3\text{H}_4$, ${}^3\text{P}_0 \rightarrow {}^3\text{H}_5$, ${}^3\text{P}_0 \rightarrow {}^3\text{F}_3$, and ${}^3\text{P}_0 \rightarrow {}^3\text{F}_3$ transitions, respectively. This observation is in agreement with the Judd-Ofelt calculation result that these transitions possess larger branch ratios than those transitions terminating to other levels. The recorded visible PL spectra show similar altering tendency as the broadband near-IR emission; they decrease after an initial increase with the further increment of Pr^{3+} in concentration. The mechanism responsible for this can be attributed to the cross relaxation process [${}^3\text{P}_0, {}^3\text{H}_4$] \rightarrow [${}^1\text{D}_2, ({}^3\text{H}_6, {}^3\text{F}_2)$], higher Pr^{3+} dopant concentration enables an easy occurrence of this process, leading to a population of the broadband emission level ${}^1\text{D}_2$. The less population of Pr^{3+} : ${}^3\text{P}_0$ results in a decreasing change of the visible emissions.

It can be observed in Fig. 4 that the blue wavelength emission gives a deeper decrease than the green and red emissions although they originate from the common level ${}^3\text{P}_0$. This means that some other quenching mechanism occurred on the Pr^{3+} : ${}^3\text{P}_0 \rightarrow {}^3\text{H}_4$ emission. Considering the spectral overlap between the high-energy emission side and the low-energy absorption side of Pr^{3+} : ${}^3\text{P}_0 \leftrightarrow {}^3\text{H}_4$, some energy in the higher sub-levels of Pr^{3+} : ${}^3\text{P}_0$ can be absorbed by a nearby Pr^{3+} in the ground state when they are in a close separation, resulting in a depletion of the higher energy sub-levels of Pr^{3+} : ${}^3\text{P}_0$. This is confirmed by the changes involved in the emission peak wavelength that presents a red-shift from 485 to 495 nm in this process, as shown in Fig. 4 inset (a). In addition, the transition from the ${}^3\text{P}_1$ to ${}^3\text{H}_4$ may contribute to this blue emission considering the observation of a shoulder around 470 nm which decreases with the increasing of Pr^{3+} concentration and nearly to be completely quenched when it reaches 1.0 mol%. This can be attributed to the process [${}^3\text{P}_1$ - ${}^3\text{H}_4$]: [${}^3\text{H}_4$ - ${}^3\text{P}_0$], taking into account that Pr^{3+} : ${}^3\text{P}_0$ shows intense absorption around 470 nm [see Fig. 4 inset (a)]. It should be also noted that the shoulder at the short wavelength side of the 613 nm emission, which has been demonstrated due to the hypersensitive Pr^{3+} : ${}^3\text{P}_1 \rightarrow {}^3\text{F}_3$ transition [31], shows a similar decrease tendency as the shoulder around 470 nm. This can be ascribed to the cross relaxation [${}^3\text{P}_1, {}^3\text{H}_4$] \rightarrow [${}^3\text{H}_6, {}^1\text{D}_2$], by which some of Pr^{3+} in ${}^3\text{P}_1$ non-radiatively decay to ${}^3\text{H}_6$ with the energy being absorbed by Pr^{3+} ions in the ground state. The matched energy difference, as shown in

inset (b) of Fig. 4, enables an easy occurrence of this process especially at higher Pr^{3+} doping level. The above explanations are also confirmed by the lifetime changes of the $^3\text{P}_0$ and $^1\text{D}_2$ states; the both decrease as the increment of Pr^{3+} in concentration, as shown in Figs. 5(a) and 5(b) and the insets of them. The lifetime values are determined using $\tau_m = \int t\varphi(t) / \int \varphi(t)$, where $\varphi(t)$ is the dependence of decay curve on the time t [30], since the decay curves show a slight deviation from the single exponential function. All the aforementioned energy transfer processes together with the excitation routes are schematically illustrated in Fig. 6.

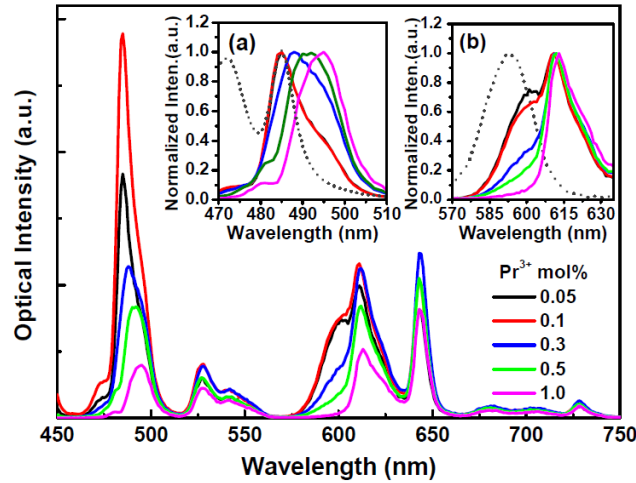


Fig. 4. Visible PL spectra of Pr^{3+} -doped fluorotellurite glasses under 445 nm excitation. Emission bands located around 490, 528, 611, and 643 nm correspond to the Pr^{3+} transitions of $(^3\text{P}_1, ^3\text{P}_0) \rightarrow ^3\text{H}_4$, $^3\text{P}_0 \rightarrow ^3\text{H}_5$, $(^3\text{P}_1, ^3\text{P}_0) \rightarrow ^3\text{H}_6$, and $^3\text{P}_0 \rightarrow ^3\text{F}_2$, respectively. Inset (a) compares the peak wavelengths of Pr^{3+} : $(^3\text{P}_1, ^3\text{P}_0) \rightarrow ^3\text{H}_4$ emission at different Pr^{3+} dopant concentration (solid lines) as well as the absorption band corresponding to Pr^{3+} : $(^1\text{I}_6 + ^3\text{P}_1, ^3\text{P}_0) \leftarrow ^3\text{H}_4$ (dotted line). Inset (b) shows the normalized PL intensity from the Pr^{3+} : $(^3\text{P}_1, ^3\text{P}_0) \rightarrow ^3\text{H}_6$ emission (solid lines) and the absorption band from the Pr^{3+} : $^1\text{D}_2 \leftarrow ^3\text{H}_4$ transition (dotted line).

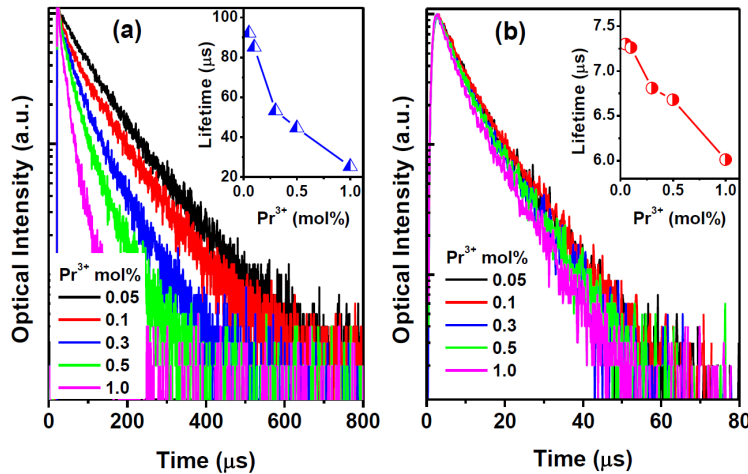


Fig. 5. Decay curves of Pr^{3+} -doped glass samples monitored at (a) 1480 nm and (b) 495 nm. Insets (a) and (b) show the lifetimes of the both emissions as a function of Pr^{3+} dopant concentration.

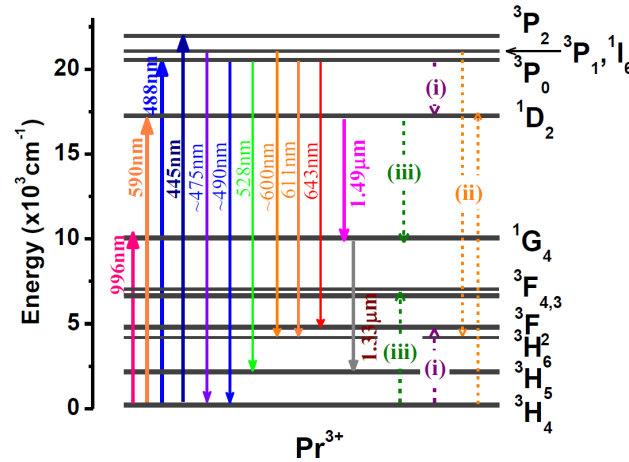


Fig. 6. Schematic energy-level diagram of Pr^{3+} in fluorotellurite glass and energy transfer processes involved. Notations (i), (ii), and (iii) stand for the cross relaxation processes [$^3\text{P}_0, ^3\text{H}_4 \rightarrow ^1\text{D}_2, (^3\text{H}_6, ^3\text{F}_2)$], [$^3\text{P}_1, ^3\text{H}_4 \rightarrow ^3\text{H}_6, ^1\text{D}_2$], and [$^1\text{D}_2, ^3\text{H}_4 \rightarrow ^1\text{G}_4, ^3\text{F}_{4,3}$] among Pr^{3+} ions, respectively.

To further evaluate the gain performance of this glass system, it is of significance to determine the stimulated emission cross-section σ_{em} . Considering that the Pr^{3+} near-IR emission occurs between two excited states, the profiles of σ_{em} can be described by the equation [28]:

$$\sigma_{em}(\lambda) = \frac{A_j \beta_{ji} \lambda_{ji}^5 I(\lambda_{ji})}{8\pi c n^2 \int \lambda_{ji} I(\lambda_{ji}) d\lambda}, \quad (2)$$

where c is the light speed in vacuum, λ_{ji} is the wavelength of a given transition from j to i which leads to the fluorescence $I(\lambda_{ji})$. Here, $A_j \beta_{ji} = 880.1 \text{ s}^{-1}$ for the $\text{Pr}^{3+}: ^1\text{D}_2 \rightarrow ^1\text{G}_4$ transition according to the Judd-Ofelt calculation. The peak value of σ_{em} is obtained to be $0.90 \times 10^{-20} \text{ cm}^2$ at 1487 nm. This value is larger than that in bismuth gallate glass and of Ni^{2+} ($0.63 \times 10^{-20} \text{ cm}^2$) in glass-ceramics [44], although smaller than the bismuth doped aluminum germanate glasses ($4.435 \times 10^{-20} \text{ cm}^2$) [26] and bismuth and tantalum codoped germanium oxide glasses ($1.59 \times 10^{-20} \text{ cm}^2$) [45]. The production $\sigma_{em} \tau_m$ is obtained to be $8.31 \times 10^{-26} \text{ cm}^2 \text{ s}$, which is proportional to the amplification gain and inversed laser oscillation threshold, suggesting that this host matrix is promising for the gain media as broadband amplifiers and tunable lasers.

4. Conclusions

In conclusion, broadband NIR emissions in the wavelength region of 1.30-1.67 μm were achieved from Pr^{3+} -singly doped fluorotellurite glasses. The bandwidth (FWHM) was improved by the increase of Pr^{3+} concentration although it resulted in a quenching of the emission at higher dopant concentration. The spontaneous transition properties analyzed using the Judd-Ofelt theory indicate a stronger covalent bonding between the Pr^{3+} sites and the matrix ligand field. The results suggest that the Pr^{3+} -doped fluorotellurite glass system is promising for broadband near-IR luminescence sources and optical amplifiers/lasers operating at the expanded low-loss telecommunication transmission window. Further investigations and experiments are underway.

Acknowledgments

Y. H. Tsang acknowledges support from The Hong Kong Polytechnic University under Grants G-YH91, G-YJ20, and A-PK72. This work was supported by the Research Grants Council of the Hong Kong SAR, China, under project CityU 119708.